IEEE Access
Multidisciplinary | Rapid Review | Open Access Journal

Received 29 May 2023, accepted 19 June 2023, date of publication 28 June 2023, date of current version 7 July 2023.

Digital Object Identifier 10.1109/ACCESS.2023.3290907

RESEARCH ARTICLE

Soil Surface Texture Classification Using RGB Images Acquired Under Uncontrolled Field Conditions

EKUNAYO-OLUWABAMI BABALOLA, MUHAMMAD H. ASAD, (Graduate Student Member, IEEE), AND ABDUL BAIS, (Senior Member, IEEE)

Department of Electronic Systems Engineering, Faculty of Engineering and Applied Science, University of Regina, Regina, SK S4S 0A2, Canada

Corresponding author: Abdul Bais (abdul.bais@uregina.ca)

This work was supported in part by Croptimistic Technology Inc., Natural Sciences and Engineering Research Council of Canada (NSERC), and MITACS; in part by the NSERC Discovery Grant through the Crop Stress Management Using Multi-Source Data Fusion under Grant RGPIN-2021-04171; in part by the NSERC Alliance Grant through the Ground Truth Validation of Crop Growth Cycle Using High-Resolution Proximal and Remote Sensing under Grant ALLRP 549723-19; and in part by the MITACS Accelerate through the Estimating Organic Matter, Soil Surface Roughness, Plant Stand Count, and Inter-Plant Spacing from High-Resolution RGB Imagery under Grant IT27704.

ABSTRACT Soil surface texture classification is a critical aspect of agriculture and soil science that affects various soil properties, such as water-holding capacity and soil nutrient retention. However, existing methods for soil texture classification rely on soil images taken under controlled conditions, which are not scalable for high spatiotemporal mapping of soil texture and fail to reflect real-world challenges and variations. To overcome these limitations, we propose a novel, scalable, and high spatial resolution soil surface texture classification process that employs image processing, texture-enhancing filters, and Convolutional Neural Network (CNN) to classify soil images captured under Uncontrolled Field Conditions (UFC). The proposed process involves a series of steps for improving soil image analysis. Initially, image segmentation is utilized to eliminate non-soil pixels and prepare the images for further processing. Next, the segmented output is divided into smaller tiles to isolate relevant soil pixels. Then, high-frequency filtering is introduced to enhance the texture of the images. Our research has shown that the Gabor filter is more effective than Local Binary Patterns (LBP) for this purpose. By creating four distinct Gabor filters, we can enhance specific, hidden patterns within the soil images. Finally, the split and enhanced images are used to train CNN classifiers for optimal analysis. We evaluate the performance of the proposed framework using different metrics and compare it to existing state-of-the-art soil texture classification frameworks. Our proposed soil texture classification process improves performance. We employed various CNN architectures in our proposed process for comparison purposes. Inception v3 produces the highest accuracy of 85.621%, an increase of 12% compared to other frameworks. With applications in precision agriculture, soil management, and environmental monitoring, the proposed novel methodology has the potential to offer a dependable and sustainable tool for classifying soil surface texture using low-cost ground imagery acquired under UFC.

INDEX TERMS Soil texture classification, image processing, convolutional neural network, uncontrolled field conditions, Gabor filter, texture enhancement.

I. INTRODUCTION

The soil particle size defines its texture. Soil textures are broadly categorized into sandy, loamy, and clayey, with further sub-classifications based on the percentage mix of sand, loam, and clay [1]. The texture of the soil surface has a significant impact on various properties such as the patterns of vegetation, water holding capacity [2], permeability, soil nutrient retention [3], porosity, and saturated hydraulic conductivity [4]. Soil texture also affects soil erodibility, soil

The associate editor coordinating the review of this manuscript and approving it for publication was Donato Impedovo.

fertility, chlorophyll levels, and plant growth [5], [6]. Clayey soils usually have high organic matter content, water retention capacity, and low permeability [7]. In contrast, sandy soils have the lowest organic matter and water retention capacity, while loamy soils lie between clayey and sandy textures [8]. Given the importance of soil texture characteristics, they are used in precision agriculture for site-specific management of soil and nutrients. Soil texture plays a crucial role in identifying Homogenized Management Zones (HMZs) for Variable Rate Application (VRA) of seeds and nutrients [9], achieving consistent crop growth, rationalizing farm inputs, and reducing environmental costs [10]. The identification of HMZs requires high-resolution mapping of soil texture.

Soil texture classification methods can be categorized into three main categories: 1) sedimentation analysis, 2) spectroscopy, and 3) image-based methods. Traditionally, soil texture is determined using lab-based sedimentation analysis methods. These methods require studying soil particle size. Bouyoucos (hydrometer) and pipette methods are common sedimentation analysis methods used to measure soil texture [11]. These methods involve soil sampling, processing, treatment, sieving, and drying [12]. The Bouyoucos method measures the size of soil particles by measuring the initial and final density of the soil in an aqueous solution [13]. The pipette method uses the weight of the soil sample to determine the soil texture [14]. Kettler et al. combine sieving and sedimentation to measure soil texture while utilizing pipette and Bouyoucos techniques [15]. Mwendwa et al. work on the Bouyoucos method and show that soils must be pre-treated with hydrogen peroxide and calgon to achieve higher accuracies [16]. These methods are time-consuming, labour-intensive, and not scalable for application in real field conditions [17]. Also, these methods are unfriendly to the environment due to the corrosive oxidizing agent used [18]. Moreover, lab-based texture mapping has low spatiotemporal resolution and does not facilitate VRA [19].

Spectroscopy is widely used for soil texture classification. Near-infrared spectroscopy is a commonly used method for soil texture analysis. This measures the energy absorption of different soil textures. Jaconi et al. use near-infrared soil spectroscopy and memory-based learning to predict soil texture [20]. Coblinski et al. expand on this by studying the performance of different spectral regions with the cubist regression algorithm for predicting soil texture [21]. Wartini et al. show that spectroscopy combined with deep learning outperforms other spectroscopy methods when sufficient data is utilized [22]. Though soil spectroscopy combined with deep learning produces promising results, it requires soil sample collection and preparation in lab settings. It is time-consuming and costly, resulting in fewer soil samples not representative of the whole field.

The recent advancements in machine learning, data storage, computer vision and image processing have led to studies investigating the potency of images to classify soil properties like Organic Matter (OM) and texture [23], [24]. This method has the advantage of being non-invasive, fast, affordable and reliable. Several image analysis methods are useful in producing reliable results for soil texture classification [25]. These can be categorized into three main groups. 1) Statistical methods based on describing image features using histogram, auto-correlation and co-occurrence matrices [26]. Sun-Ok et al. classify soil samples up to a depth of 50cm using RGB and grayscale images converted to histograms [27]. Naveed et al. apply a Gray-Level Co-occurrence Matrix (GLCM) to classify different types of crops. The GLCM extracts features from the grayscale images, which are then applied to Support Vector Machines (SVM), random forest, naive Bayes and neural networks for classification [28]. Annamalai applies GLCM on grayscale images to enhance image features and pixel information. Statistical features like contrast, correlation and homogeneity are then calculated from the GLCM and applied to K-nearest neighbour for classification [29]. Although the GLCM is very useful for classification, it has a drawback of high matrix dimensionality [30]. The statistical method of image analysis, such as the histogram and GLCM, are used to enhance important features and information in image pixels, which are vital for classification. 2) Structural methods assume image texture data appear in a spatial form. Examples include area, moments, eccentricity, elongation [31] and Local Binary Patterns (LBP) [32]. Ervin et al. use a moment invariant method and deep learning for image classification. Fusing the image moment and deep learning increases the accuracy and sensitivity of the classification process [33]. Image moment is a scalar quantity used to capture image features based on the spatial distribution of the pixels. Uddin et al. use LBP and the mean, median, and most frequent pixels for classification. The best features are selected, and then machine learning algorithms are used to classify textures into sand, silt and clay [34]. 3) Transform-based methods rely on transforming images to enhance texture data. Examples include Fourier transform [35] and Wavelets (Gabor) [36]. Gabor filters and histogram equalization are also used with SVM to classify texture [37]. Huang et al. use a Gabor filter to create a feature vector for classification using neural networks [38]. Francesco et al. discover that the smoothing property of the Gabor filter aids in its ability to transform images and enhance texture features [38]. The studies discussed above have used Gabor filters for classification due to their texture-enhancing nature. They are particularly useful in classifying images taken in UFC because of the trans-formative property of the filter. Other filters have been used for soil texture classification. Shenbagavalli et al. use the Prewitt edge filter and gray level thresholding to extract features from images for soil texture classification [39].

Various machine learning techniques effectively identify objects [40], detect patterns, and classify features [41]. In a study by Pedro et al., they developed a digital image processing workflow where RGB images are transformed into HSV. They utilized successive projections algorithm and trained

a soil texture classifier using multivariate linear regression, partial least-squares regression, and Least-Squares Support Vector Machine Regression (LSSVMR). Among these methods, LSSVMR achieved the highest accuracy of 90% [23]. Meanwhile, Wu et al. employed classification trees, Artificial Neural Networks (ANN), and SVM with polynomial and Gaussian radius basis functions to classify texture. They found that SVM with a polynomial basis function produced the best results with an accuracy rate of 94% [42].

Deep learning methods have produced impressive results for soil texture analysis. Guidang uses web images of soil samples to classify textures such as clay, sand and silt using the Inception v3 architecture with feature mining and transfer learning [43]. 2D microscopic images are acquired, and individual soil particles are captured from original particle images. The image is transformed, resized and fed into CNN models for classification. VGG-16, Inception v3 and ResNet-152 classify micro-particles into six sand particle types. Higher accuracies are observed in soil samples that are irregularly shaped and round with more distinct features [44]. In another study, dark chambers are also used to avoid light reflection, and LED strips are run through for even illumination to take other images. These images are processed further and used to classify sand and silt with random forest and CNN architectures [45]. Chandan et al. classify seven different soil types. Features like colour moments, intensity, hue, and saturation are extracted. Principal Component Analysis (PCA) and Linear Discriminant Analysis (LDA) are used to select the best features. SVM and ANN are then used to classify the texture, and SVM gives better results [46]. Utpal et al. extract features and properties from images useful for texture classification, which include HSV histogram, colour auto correlogram, colour moments and Gabor wavelets. These features are also used to train SVM and achieved an accuracy of 91.37% for soil texture classification [47].

The above methods tackle image processing and classification only using soil data collected under controlled lab conditions. The data is sieved, dried and treated for accurate results. To capture images of soil under controlled conditions, soil samples must be collected and pre-treated, but this process can be expensive and difficult to scale, leading to limited soil sampling. This creates a challenge for large farms like those in the Canadian Prairies, where the limited data gathered in a lab may not accurately represent broader field conditions. To solve this issue, our study explores the possibility of using low-cost ground images acquired through farming machinery equipped with imaging devices for soil texture classification. This approach can potentially overcome the limitations of lab-based soil sampling and produce higher-resolution soil texture maps. Under UFC, varying environmental conditions lead to blur, noise and illumination variation. The presence of vegetation, crop residue, debris, soil cover, and shadows in the soil also contributes to the poor quality of soil images and, in turn, poor results [48].

This research paper delves into the challenges of classifying soil texture in images captured under UFC. To address this problem, we propose a unique method that involves several steps to extract and process the necessary information. Firstly, we employ deep learning-based semantic segmentation to identify bare soil patches in the image, excluding vegetation, crop residue, and shadows [49]. This process generates random patches of soil pixels and zero-valued background pixels. Next, we isolate the soil pixels by dividing the image into smaller tiles. In the third step, we compare two texture-enhancing techniques, namely LBP and Gabor filters, and find that the latter performs better. Therefore, we design and combine multiple Gabor filters to enhance the texture information and increase data robustness. To maximize the information extracted, we use four different Gabor filters, each enhancing four distinct texture patterns. These filters exaggerate specific hidden textures and patterns in the soil tiles, facilitating texture classification. Finally, we combine the soil and Gabor filter images and feed them into a CNN architecture with seven channels. This architecture is designed to use fewer trainable parameters while maintaining high accuracy. We evaluated this methodology on three fields and obtained an accuracy of 80.862%. To our knowledge, this paper presents the following novel contributions in soil texture classification using Gabor filters and a CNN architecture.

- Developing soil texture classification/mapping framework using low-cost RGB images acquired under UFC.
- Using multiple Gabor filters for enhancing different textures in soil images for soil surface classification.
- Comparing the performance of Gabor filters and LBP on UFC image data.
- 12% improvement in accuracy when Inception v3 is used in our proposed process with respect to other soil texture classification frameworks.

The rest of the paper is organized as follows: Section II details methodology, Section III presents results and Section IV concludes the work and gives future research recommendations.

II. METHODOLOGY

This study proposes a scalable and sustainable method to classify soil texture using high-resolution ground-level field images taken under UFC. The basic challenge of images taken in UFC is unwanted features that disrupt soil texture information. Four steps are used in this study to classify these types of images. The first step is to extract soil pixels from high-resolution ground field images taken under UFC. Semantic segmentation is used to tackle this problem. This method removes vegetation, soil cover, shadows and crop residue. The predicted mask from the semantic segmentation step eliminates unwanted pixels from the image. This produces images of size 1440×1080 that contain soil pixels and background zero pixels. The combination of soil and zero pixels creates random patterns in the image that disturb the image texture data. The second step splits this image of size

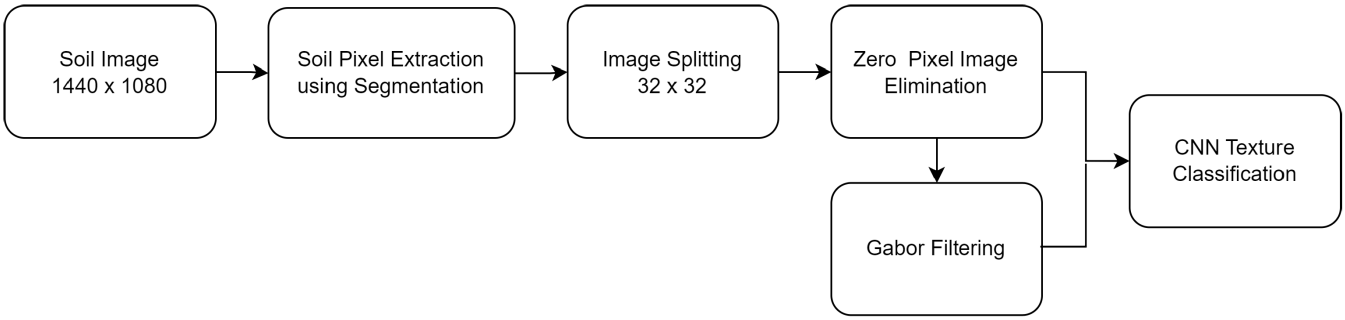

FIGURE 1. Flowchart of soil texture classification from images taken under uncontrolled field conditions.

1440 × 1080 into smaller tiles of 32 × 32 pixels. This is done to isolate soil pixels from 0 pixels values and eliminate the random patterns in the image. The resulting 32 × 32 image contains 1024 pixels. After splitting, images containing more than 24 zero-pixel values are eliminated. The third step is to enhance soil texture information from the split soil images using image analysis methods. In this study, we use two different methods and compare them to select the best. LBP and Gabor filters are compared, and the Gabor filters are selected based on their higher performance. This texture enhancement produces a new image with the same dimension, 32 × 32. Finally, the soil and texture-enhanced images are concatenated and fed into the CNN architecture. Figure 1 is the flowchart describing the proposed methodology.

A. DATA ACQUISITION

The research study is conducted in the Canadian Prairies. The images were acquired in 2021 and 2022 by Croptimistic Technology Inc. using a Samsung SM-G973W camera mounted on ground moving farm machinery from three fields. Each image is of dimension 1440 × 1080. To validate our proposed methodology, soil samples are collected from corresponding fields of study and soil texture is classified in a lab. Table 1 summarizes the number of images acquired from each field and ground truth data samples used in this study. Figure 2 shows the image data points for Field-1 and its sampled points. Images of the soil surrounding each sampled point location are collected for ground truth data. These images are used to train and validate the soil texture model. To find the surrounding images of the sampled points, we use the K-nearest neighbour algorithm selecting the five nearest neighbours for each data point.

TABLE 1. RGB image obtained from a camera mounted on ground moving farm machinery and soil sample points for each field.

Fields	Number of images	Soil sampled points
Field-1	3237	15
Field-2	3318	15
Field-3	1177	12

B. DATA CLASSIFICATION

Three different fields are utilized in this study. These fields are merged and divided into 3 different classes to create a single texture classification model. Table 2 shows all 3 classes and their respective textures. Class 0 is made of Clay and Silty Clay Loam. Class 1 is made of Loam and Clay Loam. Class 2 contains Sand, Sandy Loam, Loamy Sand and Sandy Clay Loam. Figure 3 shows the texture triangle and the 3 different classes trained. Class 0 is made of 60-100% clay. Class 1 lies in the middle of the triangle and is a mixture of 20-68% of sand, 55-80% clay, and 0-50% silt particles. Class 2 is made of 42-100% sand particles. Class 0 (60-100% Clay) has a total of 75 images, Class 1(Loam) has 75 images, and Class 2(42-100% Sand) has 60 images.

TABLE 2. Three texture classes.

Class 0 (60-100% Clay)	Class 1(Loam)	Class 2 (42-100% Sand)
Clay	Loam	Sand
Silty Clay Loam	Clay Loam	Loamy Sand
		Sandy Clay Loam

C. SOIL PIXEL SEPARATION

Once the images are sorted into their respective classes, the initial step in image processing involves semantic segmentation. Soil images captured under UFC often have elements such as vegetation, shadows, and crop residue, which make it challenging to classify the soil image texture accurately. To overcome this difficulty, semantic segmentation is employed, which involves eliminating all non-soil pixels. This technique helps isolate soil information and prepares the data for proper soil texture classification.

1) Data Labelling: Firstly, bare soil pixels are labelled. The soil pixels with shadows, vegetation, soil cover and crop residue are excluded and labelled as background, while the remaining soil pixels are labelled as soil class. The labelled data is augmented to increase the dataset and create image variation for changing field conditions. The data is augmented using rotation, blurring, scaling, cropping, and horizontal and vertical flipping.
2) Semantic Segmentation Model: CNN is a deep learning algorithm for visual imagery. It is used to carry out classification, segmentation and object detection. Semantic segmentation is used in this study for binary classification between soil pixels and background. A semantic segmentation model is made up of an encoder and a

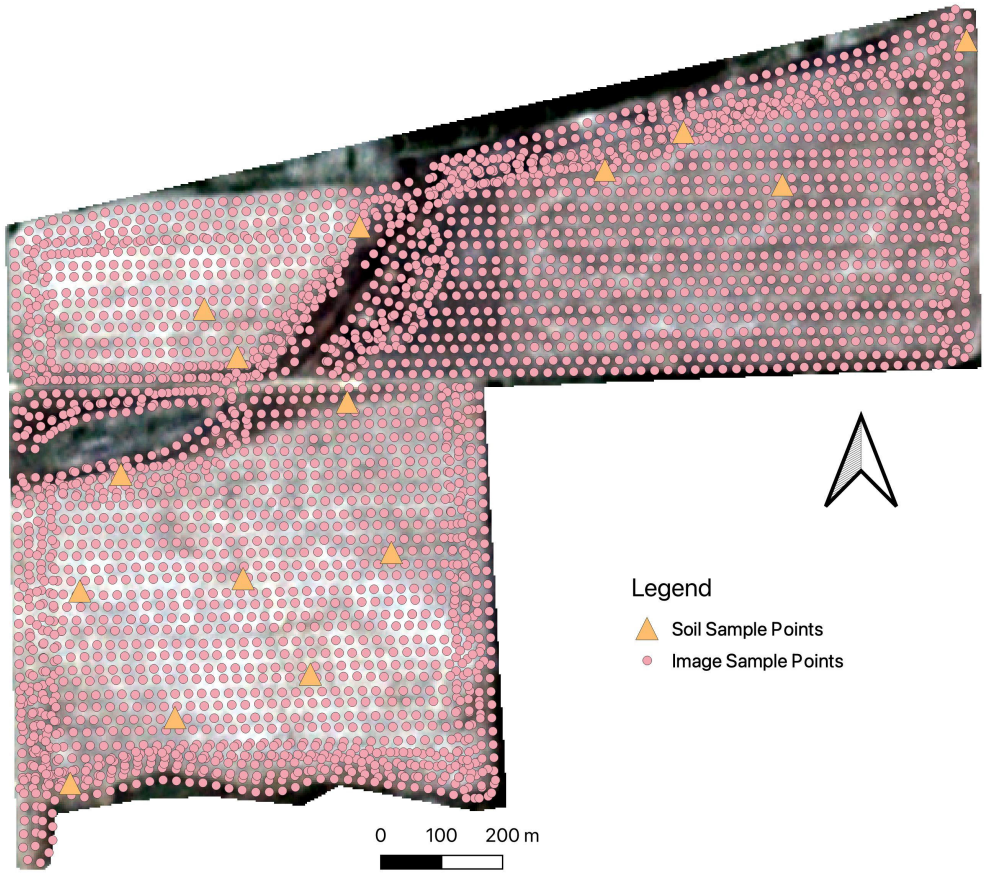

FIGURE 2. Image points and 15 soil sampled points for Field-1.

decoder. The encoder is used for deep feature extraction. The decoder is used to up-sample the results of the encoder back to the original image dimension. This results in the segmentation map. ResNet-50 [41], UNet [51], PSPNet [52], SegNet [49], [53] and DeepLab v3 [54], [55] are used to carry out semantic segmentation. Their accuracies are compared, and the best model is chosen.

The encoder block selected for this study is the ResNet-50 architecture. ResNet-50 is a CNN architecture with 50 layers. It is formed by stacking residual blocks together. It addresses the vanishing gradient problem of deep networks by using skip connections to preserve information across the layers. This preserves information learned earlier in the model. This network uses 3×3 convolutions, 7×7, 3×3 and 1×1 kernels with a stride of 2.

The ResNet-UNet architecture uses the ResNet-50 as the encoder and feature extractor. The UNet is a U-shaped model with the encoder on the left side and the decoder on the right. The decoder uses 2×2 transpose convolutions, 3×3 convolutions and ReLu activation functions. The transpose convolution is used to increase precise localization. Features from the encoder are concatenated with corresponding decoder features to preserve information. PSPNet is also divided into encoder and decoder but uses dilated convolutions and pyramid parsing to capture the entire context of an image. The pyramid poolings are of dimensions 1×1, 2×2, 3×3 and 6×6. The decoder comprises convolution layers and an $8\times$ bi-linear up-sampling layer. This up-sampling layer helps produce a segmentation output with equal dimensions to the input. The SegNet architecture uses the ResNet-50 encoder. The decoder is designed to produce sparse feature maps of high resolution. It does this by storing pooling indices from its corresponding encoder blocks. DeepLab v3 uses Atrous Separable Convolution that combines Point-wise and Depth-wise convolutions. Point-wise convolution uses a filter size of 1×1 to change the image dimensions. Depth-wise convolution uses a filter $a \times b$ on all the input channels [56].

D. IMAGE SPLITTING

Following the soil segmentation process, the resulting image may have numerous 0-pixel values that create irregular patterns in field images. These patterns have a significant impact on image texture information. To address this challenge, the images are divided into smaller tiles of 32×32 pixel values. Through experimentation, this tile size has been selected to capture maximum soil information and eliminate 0-pixel values from the image. The split images contain 1024 pixels,

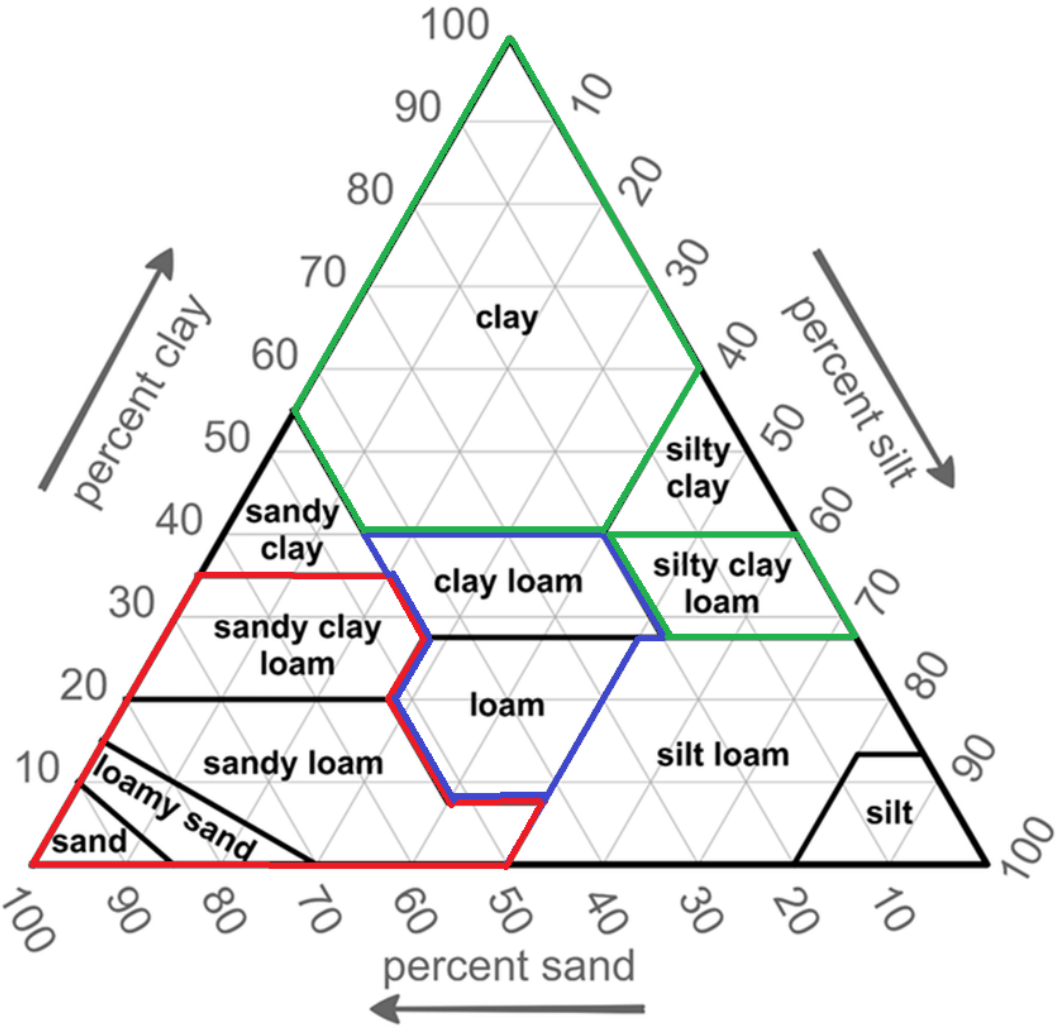

FIGURE 3. Texture Triangle [50] shows the 3 classes.

and any images containing zero pixel values greater than 24 pixels are discarded. After the split, Class 0 (60-100% Clay) had 2295 images, Class 1 (Loam) had 2315 images, and Class 2 (42-100% Sand) had 2298 images. A bar chart in Figure 4 illustrates the number of images for each class utilized for training, testing, and validation.

E. SOIL TEXTURE ENHANCEMENT

In this step, we carry out image analysis for texture enhancement and two different methods are used. The processing time, properties and resulting accuracy are compared, and the best texture-enhancing method is selected. The first method uses Gabor filters, and the second uses LBP to define texture information.

1) Method I: The Gabor filters are defined using a sinusoidal signal modulated by a Gaussian wave. It performs the function of a bandpass filter that permits only frequencies of a certain band to pass through. (1) expresses the wave modulation.

$$g(x, y; \lambda, \theta, \psi, \sigma, \gamma) = \exp\left(-\frac{x^{2\prime} + \gamma^2 y^2}{2\sigma^2}\right) \exp\left(\mathrm{i}\left(2\pi\frac{x'}{\lambda} + \psi\right)\right) \quad (1)$$

$$x' = x\cos\theta + y\sin\theta \& y' = -x\sin\theta + y\cos\theta \quad (2)$$

λ (Lambda): wavelength of sinusoidal factor
θ (Theta): orientation of normal to parallel stripes
γ (Gamma): aspect ratio
ψ: Phase offset of
σ: Sigma To design each filter, the values of the above parameters were tuned and selected. Each variable is designed to highlight different texture patterns of the image. Table 3 shows the various values selected for each Gabor filter parameter.

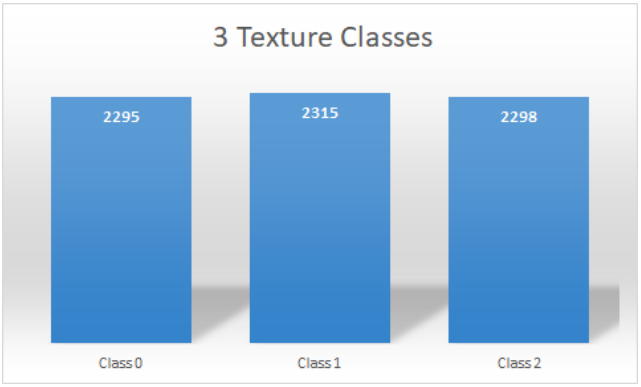

FIGURE 4. Bar chat showing the number of training images for each class.

TABLE 3. Gabor filter parameters.

Parameters	Filter 1	Filter 2	Filter 3	Filter 4
kernel size	15	15	25	40
sigma (σ)	5	4	4	5
phase offset	0.8	0.8	0.8	0.8
lambda(λ)	$\frac{\pi}{4}$	$\frac{\pi}{4}$	$\frac{\pi}{4}$	$\frac{\pi}{4}$
aspect ratio (γ)	0.9	0.9	0.9	0.9
orientation or theta (θ)	$\frac{\pi}{3}$	$\frac{\pi}{2}$	$\frac{\pi}{2}$	$\frac{\pi}{3}$

2) Method II: Local Binary Patterns are tools for texture descriptors and capturing local spatial pattern information. It proposes that texture can be described by an image's contrasting gray-level and local spatial patterns. First, the soil image is converted to grayscale, and the number of points, p and size of interest r are defined to determine the neighbourhood of interest. It selects a pixel and thresholds its surrounding pixels based on this pixel. Only pixel values less than the reference pixel are used to calculate the LBP value. The LBP for each point is calculated and stored in a 2D array. Figure 5 illustrates this on a fixed 3×3 pixel, and (3) expresses the calculation of LBP for a 3×3 image.
For each reference centre pixel (x_c, y_c) sampling p number of pixels in a radius r, the LBP is calculated with the (3).

$$\mathrm{LBP}_{\mathrm{P,r}} = \sum_{p=0}^{p-1} s\left(g_p - g_c\right) 2^P$$
$$s(z) = \begin{cases} 1, & z \geq 0 \\ 0, & z < 0 \end{cases} \tag{3}$$

g_p and g_c are gray level points in neighbouring p and reference center pixel c

F. TEXTURE CLASSIFICATION MODEL

Four CNN classification models are employed to conduct soil texture classification for comparison purposes.

1) A simple CNN model has been developed for soil texture architecture, aimed at efficiently extracting texture information from an image array of seven channels, including three RGB channels and four channels from each Gabor filter. Figure 6 displays the model's architecture, which underwent several network combinations to choose the best structure for the training data. The network of five layers, including 2D Conv layers, Dropout, Batch Normalization, Max Pooling, and a skip connection. The kernel size of 3×3 in a 2D convolution layer is used to detect the most important features for classification. Dropout enhances the network's robustness by randomly dropping out nodes. Batch normalization is used to manage the variance and mean of each layer. Max pooling selects the most prominent features in a feature map, producing a high level of information and reduced spatial dimensions. Skip connections are used to preserve the features learned earlier, with the output of one layer fed into the input of a subsequent layer. The output of the skip connection used in layer two is concatenated with the input of layer five to achieve feature re-usability. The hyper-parameters chosen for training are shown in Table 4.
2) ResNet 50 [41] for classification and segmentation tasks is discussed in the methodology section. ResNet is a standalone architecture that uses residual connections to propagate information from previous layers. When used for classification, it utilizes a softmax layer to determine the image's class probability distribution.
3) Inception v3 [57] is also employed in this study, combining convolutional filters of different sizes in each layer to learn diverse patterns at varying spatial resolutions. The network also uses auxiliary classifiers and regularization techniques to address the vanishing gradient problem.
4) EfficientNet [58] focuses on depth, width, and resolution scaling while minimizing computational costs and memory requirements. It achieves this by using a compound scaling factor to uniformly scale the width, depth, and resolution of the network. Width scaling increases the number of channels in conv layers, depth scaling increases the number of layers, and resolution scaling balances finer details and computational resources.

TABLE 4. Hyper-parameters for the training of CNN texture model.

Hyper-parameters	Values
Optimization Algorithm	Adam($\beta_1 : 0.9, \beta_2 : 0.99, \epsilon : 1e-7$)
Learning Rate	0.001 (decay step of 0.96)
Max Pooling	2×2, Stride 2
Hidden layers	4
Dropout rate	0.3
Batch Size	64

III. RESULTS

The proposed method above is tested on three fields. Image processing and soil texture classification models are trained

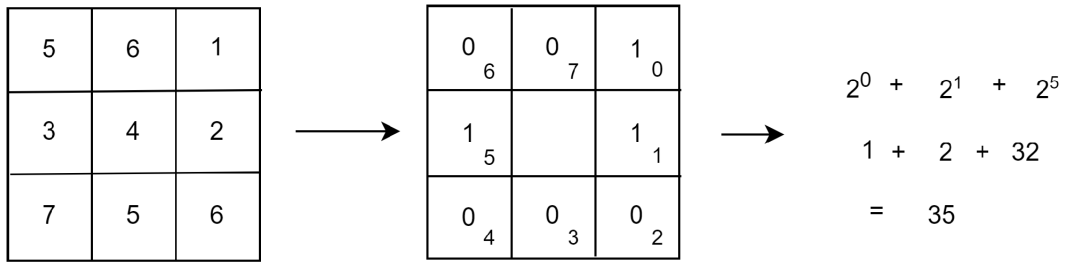

FIGURE 5. LBP on a 3 × 3 image.

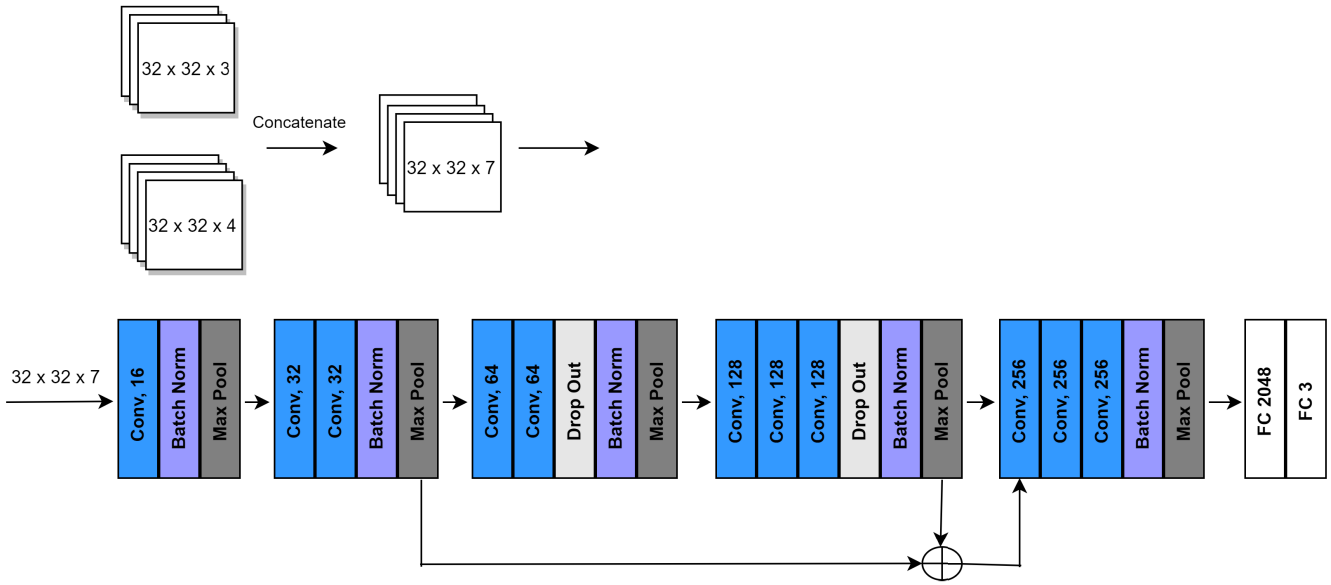

FIGURE 6. Simple CNN classifier.

and tested using a CNN classifier. The results are outlined in the following subsections:

A. MODEL EVALUATION METRICS FOR SEMANTIC SEGMENTATION

To test the models' performance, Intersection Over Union (IOU), mean IOU (mIOU), frequency-weighted IOU (fwIOU) and Dice Loss (DL) are used. DL measures the overlap between 2 sets of images. The two sets are predicted segments and the labelled ground truth segment. The dice coefficient is given by (III-A), where the numerator is twice the intersection of the predicted and ground truth sets. Dice loss is particularly effective because it considers information both globally and locally. The numerator takes local information into account, which is twice the intersecting pixels between predicted and ground truth sets while the denominator takes global information into account, which is the sum of total pixels for predicted and ground truth sets.

$$\mathrm{DL} = \frac{2\sum_i^N p_i g_i}{\sum_i^N p_i^2 + \sum_i^N g_i^2} \tag{4}$$

IOU calculates the degree of overlap between two image sets, the predicted and ground truth sets. It is the ratio of intersection to the union. The following equation gives the expression for IOU.

$$\mathrm{IOU} = \frac{\text{Area of Overlap}}{\text{Area of Union}} = \frac{p_i \cap g_i}{p_i \cup g_i} \tag{5}$$

p is the predicted class and g is the ground truth label.

$$\mathrm{IOU} = \frac{\mathrm{TP}}{\mathrm{TP} + \mathrm{FP} + \mathrm{FN}} \tag{6}$$

TP is the true positive, *FP* is the false positive and *FN* is the false negative. The individual IOUs are computed for the soil class and everything else, including vegetation, crop residue and shadows. To compute semantic segmentation's overall performance mean of IOUs is also estimated as provided by the following equation:

$$\mathrm{mIOU} = \frac{\mathrm{IOU_i} + \mathrm{IOU_j}}{2} \tag{7}$$

where i and j represent the 2 classes of segmentation. To address the class imbalance in evaluating model performance,

fwIOU is computed where weight is assigned to each class based on its data frequency.

$$\text{fwIOU} = w_i \times \text{IOU}_\text{i} + w_j \times \text{IOU}_\text{j} \tag{8}$$

where w_i and w_j are the weights for each class.

B. SEMANTIC SEGMENTATION RESULTS

The field images are labelled using Segments.ai. Then labelled images are pre-processed and augmented to increase the dataset for better generalization. The original image dimension of 1440 × 1080 is split into tiles of 736 × 544. The dataset is randomly split into 70:15:15 ratio for training, testing and evaluation. UNet, SegNet, PSPNet and DeepLab v3 architectures are used for semantic segmentation with ResNet-50 as an encoder block. All models are trained for 80 epochs. Figure 7 compares the training and validation loss of all 4 models. It is observed that the loss of UNet and SegNet reduces consistently.

The IOU, mIOU, fwIOU and accuracy of all trained models are shown in Table 5. UNet has the best IOU, mIOU and fwIOU. SegNet has the best loss and accuracy. DeepLab has shown the lowest performance, with PSPNet performing slightly better. Based on these results, UNet is selected for semantic segmentation of soil and background pixels. This model produces predicted masks containing 2-pixel values. The pixels for soil are kept at one, and the pixels for the background are kept at zero. This zero and one mask is combined with all original images to remove all unwanted background pixels and retain just soil pixels. Figure 8a contains soil images before segmentation and Figure 8b after semantic segmentation.

C. TEXTURE ENHANCING

In this study, the accuracy of LBP and Gabor filters is compared. Gabor filtering combines various aspects such as wavelengths, aspect ratios, orientation, phase, and sigma values, and four specific filters are designed to enhance soil image texture. To demonstrate the effectiveness of Gabor filters, snippets of eight texture images are presented in Figure 9 and Figure 10 after applying Gabor Filter-1 and Gabor Filter-3. Interestingly, the same images are used for both figures. Figure 9a shows a snippet of Loamy (70-100% sand) texture images after Filter-1 is applied, and Figure 10a shows the same texture images after Filter-3 is applied. Similarly, Figure 9b displays a snippet of Sandy Loam (<70% sand) texture images after Filter-1 is applied, and Figure 9b presents the same texture images after applying Filter-3. It is worth noting that Filter-1 and Filter-3, although applied on the same image loam and sand images, highlight distinct texture patterns. Moreover, we observe that the texture patterns of loamy soils differ significantly from those of sandy soils. Overall, the texture-enhancing properties of the different Gabor filters make them highly valuable for this study. Table 6 compares the accuracy of the CNN model when the soil images are used alone and with the combination of LBP and Gabor filtering. It is observed that the CNN model trained on soil segment images alone produces an accuracy of 79.022%, and the CNN model trained on soil images and LBP enhancing methods produces an accuracy of 83.782%. However, the model using our proposed enhancing framework with Gabor filters produces the highest accuracy of 85.621%, so we select the Gabor filters as our texture-enhancing method. We also use Shannon's entropy to measure the effectiveness of Gabor filters and LBP in enhancing image texture. Shannon's entropy [59]is a valuable tool in image processing because it can determine the complexity, noise level, and amount of information in an image.

$$H(X) = -\sum(P(x)\log_2(P(x))) \tag{9}$$

where H(X) is Shannon's Entropy

P(x) is the probability of pixel x occurring and

$\sum$ is used to sum over all possible pixel values.

A higher entropy score indicates an image is more complex, noisy, and unpredictable. We applied Shannon's entropy to two original images and analyzed the results. In Figure 11, we calculated the entropy of the raw image, Gabor-filtered image, and LBP image. In Figure 11a, the entropy of the original image was 9.3506, while the entropy after applying LBP was 6.4814, and after applying Gabor Filter-1, it was 4.5822. Similarly, in Figure 11b, the entropy of the original image was 9.4989, while the entropy after applying LBP was 6.2859, and after applying Gabor Filter-1, it was 5.0546.

D. MODEL EVALUATION METRICS FOR TEXTURE CLASSIFICATION

To evaluate the models' performance for texture classification, we use Accuracy, F1 score, Precision and Recall. Accuracy provides a general assessment of the performance of a model by calculating the ratio of predictions to the total number of predictions. It provides us with information on how close the predictions are to the true ground truth data.

$$\text{Accuracy} = \frac{\text{TP} + \text{TN}}{\text{TP} + \text{TN} + \text{FP} + \text{FN}} \tag{10}$$

where *TP* is the true positive, *TN* is the true negative, *FP* is the false positive and *FN* is the false negative. Precision measures the number of positive predictions predicted positively and compares this with all the positive predictions for that class. It particularly helps us avoid false positives.

$$\text{Precision} = \frac{\text{TP}}{\text{TP} + \text{FP}} \tag{11}$$

Recall measures the number of positive predictions that are accurately predicted. It particularly helps us avoid false negatives. It's also known as the sensitivity of the true positive rate.

$$\text{Precision} = \frac{\text{TP}}{\text{TP} + \text{FN}} \tag{12}$$

The F1 score combines precision and recall to provide a balanced metric to evaluate the model's performance.

$$\text{F1score} = \frac{2 \times (\text{Precision} \times \text{Recall})}{\text{Precision} + \text{Recall}} \tag{13}$$

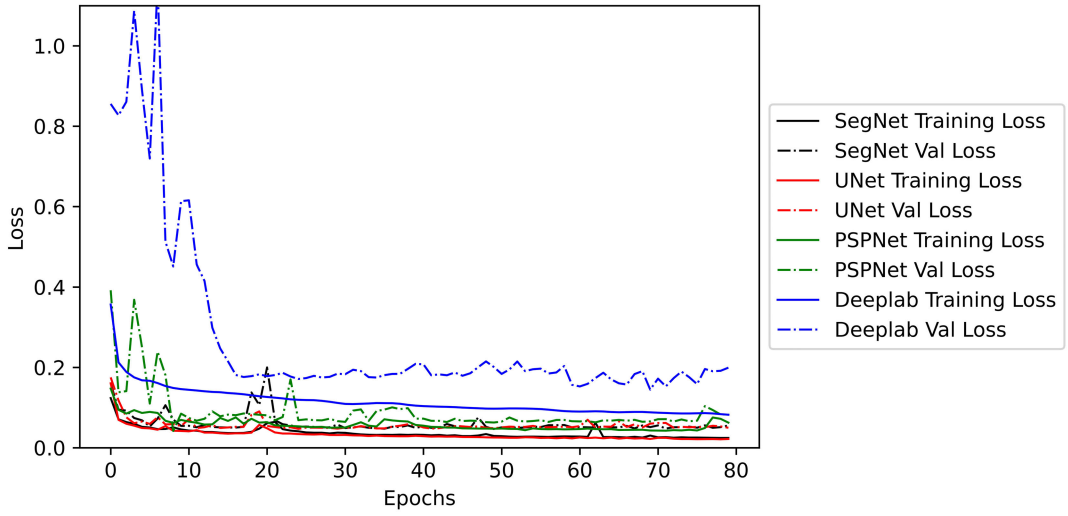

FIGURE 7. Training and validation loss of deep learning models for semantic segmentation.

TABLE 5. Semantic segmentation result on test data for soil pixel separation.

Models	Accuracy	DL	IOU Background	IOU Soil pixel	mIOU	fwIOU
SegNet_ResNet 50	**0.9297**	**0.0445**	0.91089	0.71244	0.81166	0.86956
UNet_ResNet 50	0.9252	0.0459	**0.91197**	**0.72075**	**0.0.81636**	**0.86991**
PSPNet_ResNet 50	0.9072	0.0727	0.89736	0.67709	0.78723	0.83160
DeepLab v3+	0.9055	0.1018	0.86627	0.65107	0.75867	0.82807

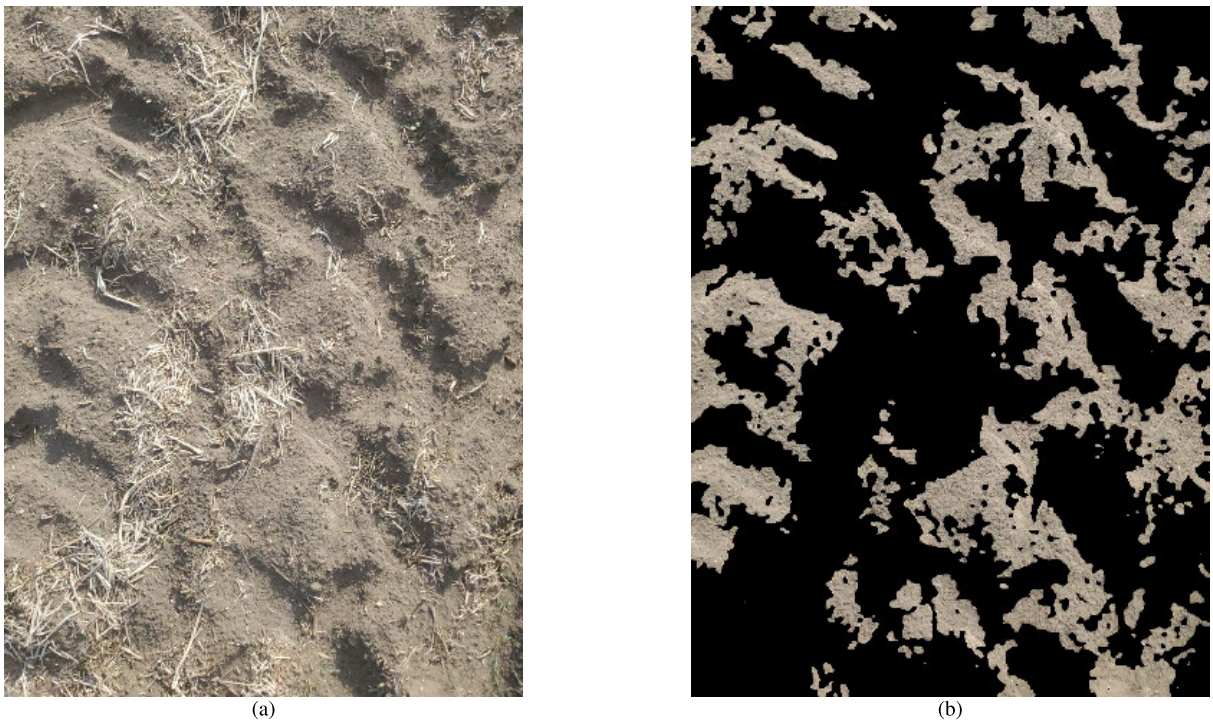

(a) (b)

FIGURE 8. (a) is the original image and (b) is the predicted image of the semantic segmentation model.

E. TEXTURE CLASSIFICATION RESULTS

For our training process, we utilize 70% of the processed ground truth data, while 15% is allocated for validation and testing, respectively. The texture classifier operates using split and Gabor-filtered images for classification. We train all 4 CNN models for 100 epochs and compare their training

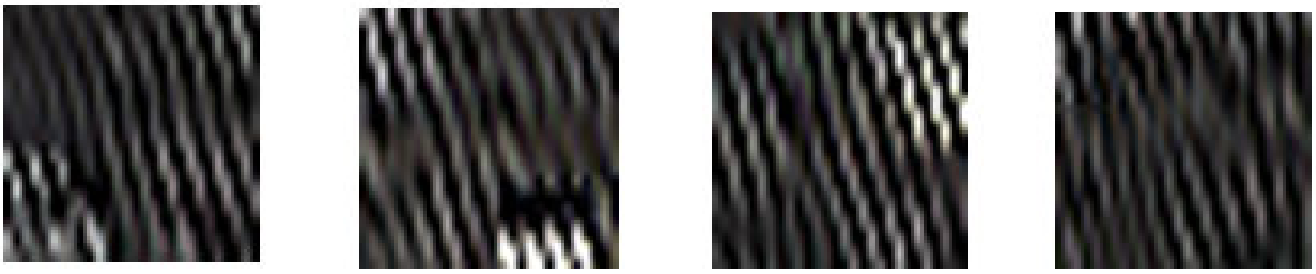

(a) Loamy Sand after Gabor Filter-1

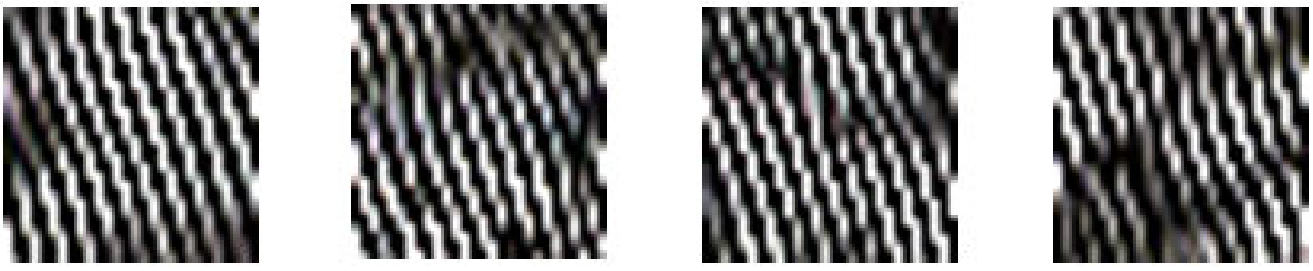

(b) Sandy Loam after Gabor Filter-1

FIGURE 9. Comparing the output of Gabor texture enhancing filter 1 for Loamy Sand and Sandy Loam soils.

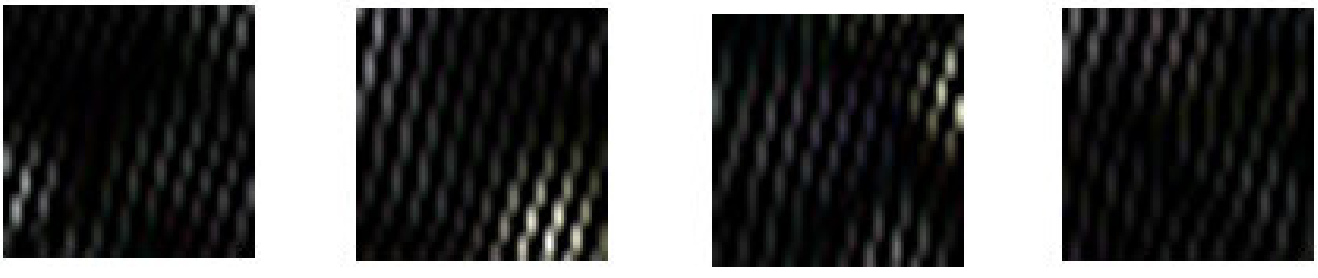

(a) Loamy Sand after Gabor Filter-4

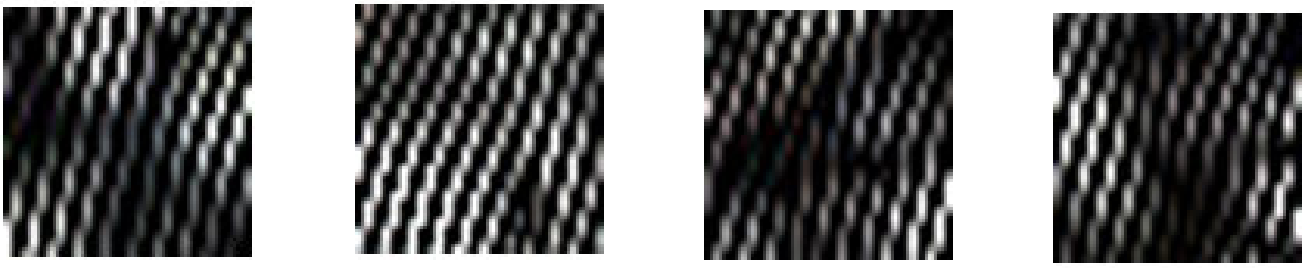

(b) Sandy Loam after Gabor Filter-4

FIGURE 10. Comparing the output of Gabor texture enhancing Filter-4 for Loamy Sand and Sandy Loam soils.

TABLE 6. Accuracy when LBP and Gabor filters are implemented.

Model Input	Accuracy
Image + Gabor	**0.85621**
Image + LBP	0.83782
Image	0.79022

and validation accuracy in Figure 12. Our texture classifier achieves the highest accuracy of 85.621% on the test dataset. We process the remaining data similarly to the ground truth data to obtain predictions. Each split tile from the 32×32 tiles extracted from the 1440×1080 image is named with a unique identifier, including the original image name, for identification purposes. We collate the predictions of all tiles for each image and select the final prediction based on the maximum predicted class of all split image tiles. This process enables us to predict soil surface texture for the entire field using RGB images, with higher spatial resolution than texture mapping based on limited soil sampling. You can see the distribution of soil and image sample points on the map in Figure 2.

(a) Original image 1, LBP image and Gabor filtered image

(b) Original image 2, LBP image and Gabor filtered image

FIGURE 11. Original Image, LBP image and Gabor filtered images 1 and 2 used to calculate Shannon's entropy.

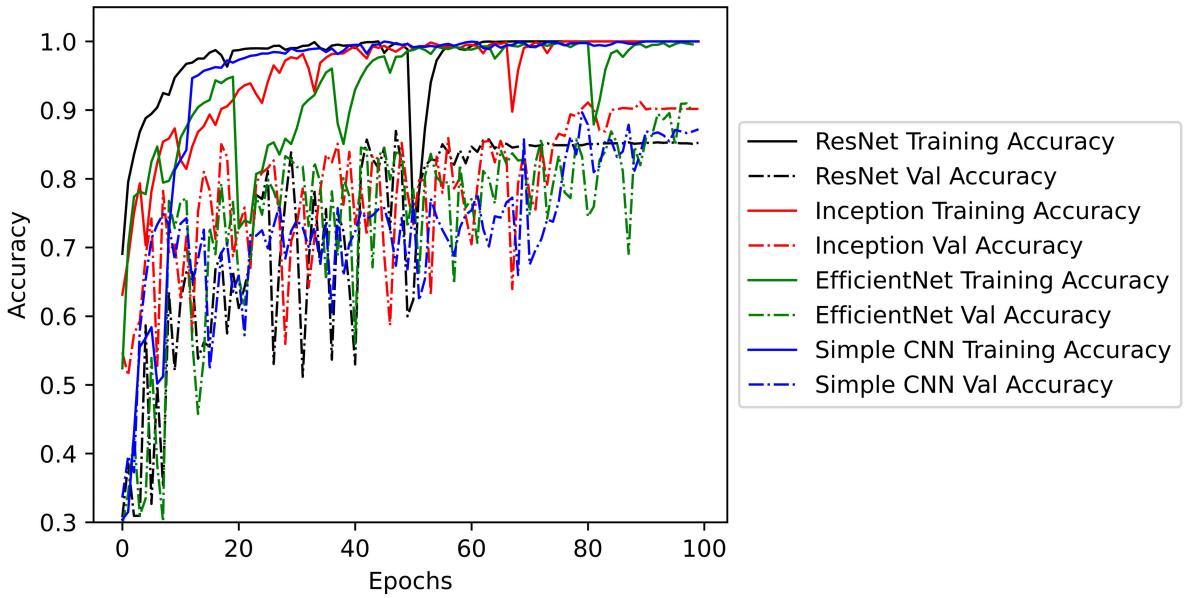

FIGURE 12. Training and validation accuracy of CNN Classification model.

We also take several steps to compare our model with the existing state-of-the-art models and methods for soil texture classification. We utilize these methods and apply them to our data taken under UFC. The first method we compared our results with is the LS-SVMR [23] method. This produced an accuracy of 90% when used to carry out soil texture classification on images taken under controlled conditions. The same method is replicated on our image data taken under UFC, producing an accuracy of 72.769%. The second method we studied and compared is the SVM-poly [42] method. This produces an accuracy of 94% for soil texture classification. The same method is applied to our data taken under UFC and produces an accuracy of 58.085%. The classification results for this study are analyzed in Table 7. The third section shows the results for the LS-SVMR [23] method and SVM-poly [42] method when applied to our dataset. The second section compares the accuracy of four CNN state-of-the-art methods applied to our data without the texture-enhancing framework. The first section compares the results of these methods with our proposed framework. We observe that the accuracy, f1 score, precision and recall of the CNN models combined with our texture-enhancing framework are improved. Inception v3,

TABLE 7. Texture Classification Results.

	Model	Accuracy	F1 Score	Precision	Recall
Other Frameworks	LS-SVMR [23]	0.72769	0.51179	0.51761	0.50609
	SVM-Poly [42]	0.58085	0.57975	0.57888	0.58063
Without Texture Enhancing Framework	Inception v3	0.79022	0.79603	0.80170	0.79044
	EfficientNet	0.79833	0.78394	0.79362	0.77452
	ResNet 50	0.78766	0.79500	0.80395	0.78625
	Simple CNN	0.52349	0.59464	0.70778	0.51268
With Texture Enhancing Framework	EfficientNet	0.84226	0.85063	0.85189	0.84936
	ResNet 50	0.83275	0.82835	0.83328	0.82347
	Simple CNN	0.80106	0.76845	0.78916	0.74881
	Inception v3	**0.85621**	**0.85642**	**0.85745**	**0.85538**

combined with our framework, produced the highest accuracy of 85.621%.

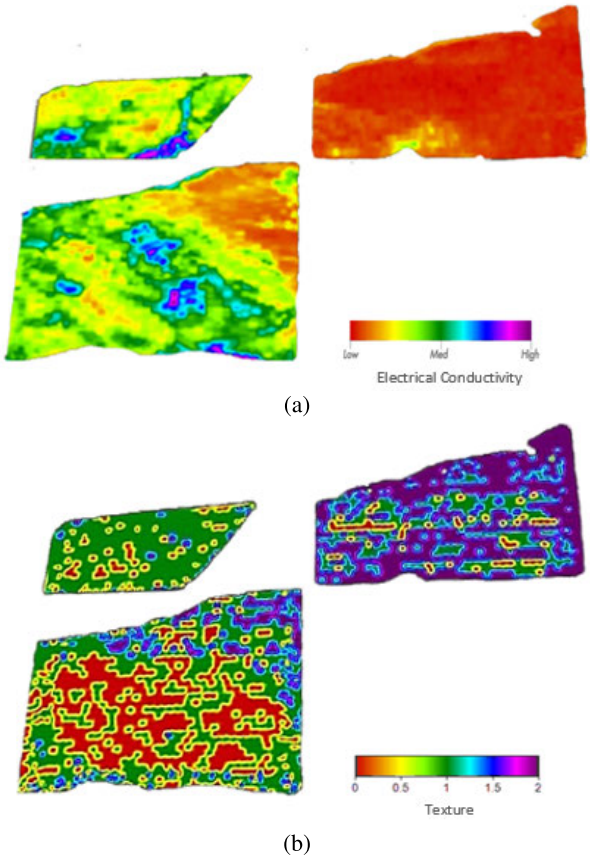

(a)

(b)

FIGURE 13. (a) is the EC of Field 1 (b) is the predicted texture.

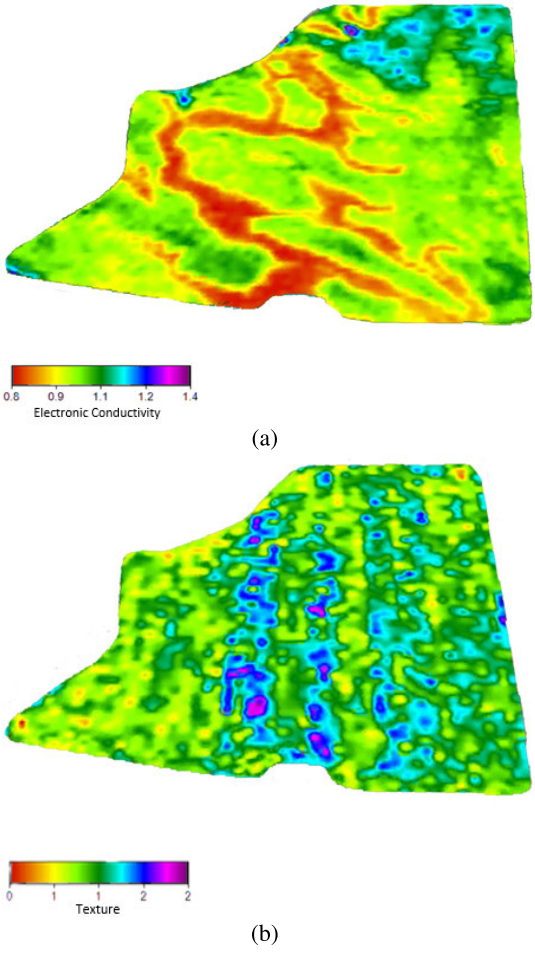

(a)

(b)

FIGURE 14. (a) is the EC of Field 2 (b) is the predicted texture.

The soil surface texture map for the fields is created using the result of the predicted class. Figure 13b displays the predicted texture class for Field 1, while Figure 14b shows the predicted texture class for Field 3. To further validate and compare our results, we use soil Electric conductivity (EC) maps provided by Croptimistic Technology Inc. Soil EC measures the soil's ability to conduct current [60] and provides descriptive texture information about the field. Smaller clay particles conduct better than larger sand particles [61], resulting in high EC for clay soils (20-800mS/m), medium EC for silt (8-80mS/m), and low EC for sand (1-10mS/m) [62]. However, it should be noted that EC maps provide average soil texture up to a depth of 1 meter, while generated soil texture maps provide soil surface texture. As a result, we compare generated soil texture maps and EC maps to identify similarities. Figure 13a and Figure 14a display the EC maps for Field 1 and Field 3, respectively.

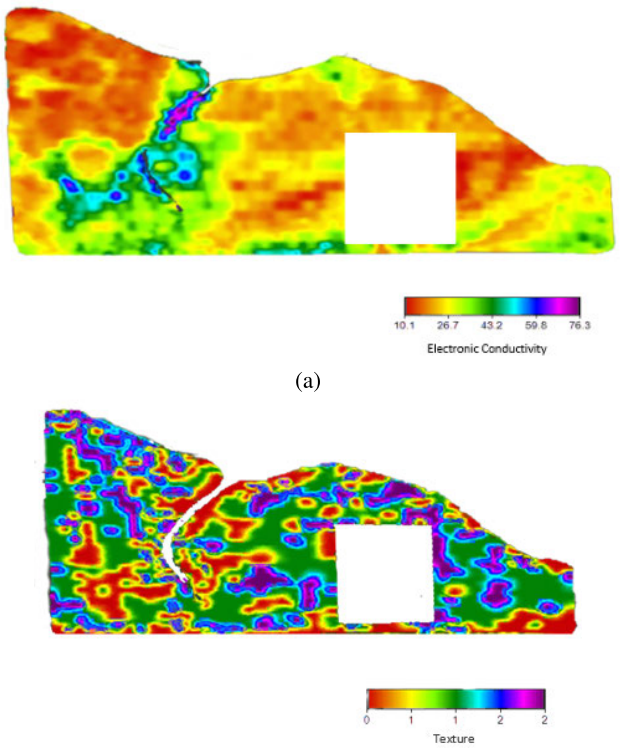

FIGURE 15. (a) is the EC of Field 3 (b) is the predicted texture.

In Field 1, we observe that the North East region has low EC soils with low moisture and salt content. This corresponds to the northeast region of the texture map, which has coarser particles represented by class 2 (Sandy soils). The mid-south region of Field 1 contains high EC soils with higher water and soil content, corresponding to the higher concentration of finer soil particles predicted as class 0 (Clayey soil) in the mid-south region of the texture map (Figure 13b). Loam soils transition from sand to clayey soils, with mid-EC values. Similar patterns are observed in Figure 14 and Figure 15. However, there may be differences between EC and predicted texture maps since EC provides insight into average soil texture up to a depth of $1m$, whereas predicted soil texture using RGB images maps soil surface texture. Soil texture can change with depth. Overall, our predicted texture map and EC map exhibit general similarities, highlighting the validity of our developed methodology. We observe some streakiness in the generated texture maps shown in Figure 13b, Figure 14b, and Figure 15b. This is due to changing ambient lighting conditions during RGB image acquisition. Further research is needed to correct images for changing ambient conditions during image acquisition.

IV. CONCLUSION

In this study, we proposed a method for accurately classifying soil texture in images captured under UFC. Due to the complexity of the images, we utilize various image processing techniques to eliminate unwanted information. Our approach involves semantic segmentation, where we compare different methods and determine UNET-ResNet-50 as the most effective. The output of the semantic segmentation is then split into smaller tiles, and texture-enhancing filters are applied to selected tiles using Gabor filters for increased accuracy. We design four Gabor filters highlighting various soil patterns in each image, increasing data robustness. The images are then fed into a CNN texture classifier, which significantly improves the accuracy of the state-of-the-art architecture, Inception v3, from 79.022% to 85.621%, a 7.696% increase. We also generate texture maps for validation, which we compare to EC maps that provide soil information up to $1m$ depth. Our soil texture maps closely resemble the distribution pattern in EC maps, although further research is necessary for images captured under changing ambient lighting conditions. It is important to note that EC maps cannot be considered ground truth for soil texture as they provide soil information up to $1m$ depth, whereas generated soil texture maps only provide surface soil texture.

ACKNOWLEDGMENT

The authors would like to thank the industry partnership with Croptimistic Technology Inc., which provided them with the necessary data and domain expertise.

REFERENCES

[1] A. Gerakis and B. Baer, "A computer program for soil textural classification," *Soil Sci. Soc. Amer. J.*, vol. 63, no. 4, pp. 807–808, Jul. 1999.
[2] C. P. Fernandez-Illescas, A. Porporato, F. Laio, and I. Rodriguez-Iturbe, "The ecohydrological role of soil texture in a water-limited ecosystem," *Water Resour. Res.*, vol. 37, no. 12, pp. 2863–2872, Dec. 2001.
[3] Q. Xia, T. Rufty, and W. Shi, "Soil microbial diversity and composition: Links to soil texture and associated properties," *Soil Biol. Biochem.*, vol. 149, Oct. 2020, Art. no. 107953.
[4] J. Van den Akker and B. Soane, "Compaction," in *Encyclopedia of Soils in the Environment*. Amsterdam, The Netherlands: Elsevier, 2005.
[5] K. Chakraborty and B. Mistri, "Importance of soil texture in sustenance of agriculture: A study in Burdwan-I CD Block, Burdwan, West Bengal," *Eastern Geographer*, vol. 21, no. 1, pp. 475–482, 2015.
[6] P. R. Chaudhari, D. V. Ahire, V. D. Ahire, M. Chkravarty, and S. Maity, "Soil bulk density as related to soil texture, organic matter content and available total nutrients of Coimbatore soil," *Int. J. Sci. Res. Publications*, vol. 3, no. 2, pp. 1–8, 2013.
[7] A. Cihan, J. S. Tyner, and E. Perfect, "Predicting relative permeability from water retention: A direct approach based on fractal geometry," *Water Resour. Res.*, vol. 45, no. 4, pp. 1–8, Apr. 2009, doi: 10.1029/2008WR007038.
[8] K. H. Yusof, F. Aman, A. S. Ahmad, M. Abdulrazaq, M. N. Mohammed, M. S. Z. M. Zabidi, and M. Y. H. Sauzi, "Determination of soil texture using image processing technique," in *Proc. IEEE 18th Int. Colloq. Signal Process. Appl. (CSPA)*, May 2022, pp. 178–181.
[9] E. Šarauskis, M. Kazlauskas, V. Naujokienė, I. Bručienė, D. Steponavičius, K. Romaneckas, and A. Jasinskas, "Variable rate seeding in precision agriculture: Recent advances and future perspectives," *Agriculture*, vol. 12, no. 2, p. 305, Feb. 2022.
[10] P. Bandyopadhyay, S. Shrestha, and L. L. Nalley, "Application of precision agriculture to maize and soybean production in developing countries: A review," *Precis. Agricult.*, vol. 18, no. 3, pp. 350–369, 2017.
[11] G. J. Bouyoucos, "A comparison between the pipette method and the hydrometer method for making mechanical analyses of soil," *Soil Sci.*, vol. 38, no. 5, pp. 335–346, Nov. 1934.
[12] J. T. Elfaki, M. A. Gafer, M. M. Sulieman, and M. E. Ali, "Hydrometer method against pipette method for estimating soil particle size distribution in some soil types selected from central Sudan," *Int. J. Eng. Res. Adv. Technol.*, vol. 2, no. 2, pp. 25–41, 2016.

[13] J. Ashworth, D. Keyes, R. Kirk, and R. Lessard, "Standard procedure in the hydrometer method for particle size analysis," *Commun. Soil Sci. Plant Anal.*, vol. 32, nos. 5–6, pp. 633–642, Apr. 2001.

[14] G. W. Gee and D. Or, "2.4 Particle-size analysis," in *Methods of Soil Analysis: Part 4 Physical Methods*, vol. 5. Madison, WI, USA: Soil Science Society of America, 2002, pp. 255–293.

[15] T. A. Kettler, J. W. Doran, and T. L. Gilbert, "Simplified method for soil particle-size determination to accompany soil-quality analyses," *Soil Sci. Soc. Amer. J.*, vol. 65, no. 3, pp. 849–852, May 2001.

[16] S. Mwendwa, "Revisiting soil texture analysis: Practices towards a more accurate bouyoucos method," *Heliyon*, vol. 8, no. 5, May 2022, Art. no. e09395.

[17] L. Liu, J. Chen, P. Fieguth, G. Zhao, R. Chellappa, and M. Pietikäinen, "From BoW to CNN: Two decades of texture representation for texture classification," *Int. J. Comput. Vis.*, vol. 127, no. 1, pp. 74–109, Jan. 2019.

[18] M. Uddin, B. Joseph, and M. Hussain, "Environmental implications of the use of hydrogen peroxide and other alternative chemical products for soil and groundwater remediation," *J. Environ. Sci. Health, A*, vol. 40, no. 5, pp. 905–926, 2005.

[19] A. B. McBratney, M. L. Mendonça Santos, and B. Minasny, "Integrating digital soil mapping and soil sensing for precision agriculture," *Precis. Agricult.*, vol. 6, no. 4, pp. 377–393, 2005.

[20] A. Jaconi, C. Vos, and A. Don, "Near infrared spectroscopy as an easy and precise method to estimate soil texture," *Geoderma*, vol. 337, pp. 906–913, Mar. 2019.

[21] J. A. Coblinski, É. Giasson, J. A. Demattê, A. C. Dotto, J. J. F. Costa, and R. Vašát, "Prediction of soil texture classes through different wavelength regions of reflectance spectroscopy at various soil depths," *Catena*, vol. 189, Jun. 2020, Art. no. 104485.

[22] W. Ng, B. Minasny, W. D. S. Mendes, and J. A. M. Demattê, "The influence of training sample size on the accuracy of deep learning models for the prediction of soil properties with near-infrared spectroscopy data," *Soil*, vol. 6, no. 2, pp. 565–578, Nov. 2020.

[23] P. A. de Oliveira Morais, D. M. de Souza, B. E. Madari, and A. E. de Oliveira, "A computer-assisted soil texture analysis using digitally scanned images," *Comput. Electron. Agricult.*, vol. 174, Jul. 2020, Art. no. 105435.

[24] Z. Fan, J. E. Herrick, R. Saltzman, C. Matteis, A. Yudina, N. Nocella, E. Crawford, R. Parker, and J. Van Zee, "Measurement of soil color: A comparison between smartphone camera and the Munsell color charts," *Soil Sci. Soc. Amer. J.*, vol. 81, no. 5, pp. 1139–1146, Sep. 2017.

[25] J. M. Prats-Montalbán, A. de Juan, and A. Ferrer, "Multivariate image analysis: A review with applications," *Chemometric Intell. Lab. Syst.*, vol. 107, no. 1, pp. 1–23, May 2011.

[26] R. M. Haralick, "Statistical and structural approaches to texture," *Proc. IEEE*, vol. 67, no. 5, pp. 786–804, May 1979.

[27] S.-O. Chung, K.-H. Cho, J.-W. Cho, K.-Y. Jung, and T. Yamakawa, "Texture classification algorithm using RGB characteristics of soil images," Kyushu Univ. Library, Nishi Ward, Tech. Rep., 2012.

[28] N. Iqbal, R. Mumtaz, U. Shafi, and S. M. H. Zaidi, "Gray level co-occurrence matrix (GLCM) texture based crop classification using low altitude remote sensing platforms," *PeerJ Comput. Sci.*, vol. 7, p. e536, May 2021.

[29] A. Suresh and K. L. Shunmuganathan, "Image texture classification using gray level co-occurrence matrix based statistical features," *Eur. J. Sci. Res.*, vol. 75, no. 4, pp. 591–597, 2012.

[30] A. Ramola, A. K. Shakya, and D. Van Pham, "Study of statistical methods for texture analysis and their modern evolutions," *Eng. Rep.*, vol. 2, no. 4, p. e12149, 2020.

[31] A. Rosenfeld and B. S. Lipkin, "Texture synthesis," in *Picture Processing and Psychopictorics*. New York, NY, USA: Academic, 1970, pp. 309–345.

[32] T. Ojala, M. Pietikäinen, and T. Mäenpää, "Multiresolution gray-scale and rotation invariant texture classification with local binary patterns," *IEEE Trans. Pattern Anal. Mach. Intell.*, vol. 24, no. 7, pp. 971–987, Jul. 2002.

[33] E. G. Moung, C. J. Hou, M. M. Sufian, M. H. A. Hijazi, J. A. Dargham, and S. Omatu, "Fusion of moment invariant method and deep learning algorithm for COVID-19 classification," *Big Data Cognit. Comput.*, vol. 5, no. 4, p. 74, Dec. 2021.

[34] M. Uddin and M. R. Hassan, "A novel feature based algorithm for soil type classification," *Complex Intell. Syst.*, vol. 8, no. 4, pp. 3377–3393, Aug. 2022.

[35] B. K. Alsberg, A. M. Woodward, and D. B. Kell, "An introduction to wavelet transforms for chemometricians: A time-frequency approach," *Chemometric Intell. Lab. Syst.*, vol. 37, no. 2, pp. 215–239, Jun. 1997.

[36] P. Scheunders, S. Livens, G. Van de Wouwer, P. Vautrot, and D. Van Dyck, "Wavelet-based texture analysis," *Int. J. Comput. Sci. Inf. Manag.*, vol. 1, no. 2, pp. 22–34, 1998.

[37] S. Shivhare and K. Cecil, "Automatic soil classification by using Gabor wavelet & support vector machine in digital image processing," in *Proc. 3rd Int. Conf. Inventive Res. Comput. Appl. (ICIRCA)*, Sep. 2021, pp. 1738–1743.

[38] L.-L. Huang, A. Shimizu, and H. Kobatake, "Classification-based face detection using Gabor filter features," in *Proc. 6th IEEE Int. Conf. Autom. Face Gesture Recognit.*, May 2004, pp. 397–402.

[39] R. Shenbagavalli and K. Ramar, "Classification of soil textures based on laws features extracted from preprocessing images on sequential and random windows," *Bonfring Int. J. Adv. Image Process.*, vol. 1, pp. 15–18, Dec. 2011.

[40] J. A. R. Recio, L. A. R. Fernandez, and A. Fernández-Sarriá, "Use of Gabor filters for texture classification of digital images," *Física de la Tierra*, vol. 17, p. 47, 2005.

[41] K. He, X. Zhang, S. Ren, and J. Sun, "Deep residual learning for image recognition," in *Proc. IEEE Conf. Comput. Vis. Pattern Recognit. (CVPR)*, Jun. 2016, pp. 770–778.

[42] W. Wu, A.-D. Li, X.-H. He, R. Ma, H.-B. Liu, and J.-K. Lv, "A comparison of support vector machines, artificial neural network and classification tree for identifying soil texture classes in southwest China," *Comput. Electron. Agricult.*, vol. 144, pp. 86–93, Jan. 2018.

[43] E. P. B. Guidang, "Classifying soil texture images using transfer learning," *IOP Conf. Ser., Mater. Sci. Eng.*, vol. 482, no. 1, Mar. 2019, Art. no. 012042.

[44] Y. Kim and T. S. Yun, "How to classify sand types: A deep learning approach," *Eng. Geol.*, vol. 288, Jul. 2021, Art. no. 106142.

[45] R. K. Swetha, P. Bende, K. Singh, S. Gorthi, A. Biswas, B. Li, D. C. Weindorf, and S. Chakraborty, "Predicting soil texture from smartphone-captured digital images and an application," *Geoderma*, vol. 376, Oct. 2020, Art. no. 114562.

[46] R. Chandan, "An intelligent model for Indian soil classification using various machine learning techniques," *Int. J. Comput. Eng. Res.*, vol. 33, no. 2250, p. 3005, 2018.

[47] U. Barman and R. D. Choudhury, "Soil texture classification using multi class support vector machine," *Inf. Process. Agricult.*, vol. 7, no. 2, pp. 318–332, Jun. 2020.

[48] L. Armi and S. Fekri-Ershad, "Texture image analysis and texture classification methods—A review," 2019, *arXiv:1904.06554*.

[49] M. H. Asad and A. Bais, "Weed density estimation using semantic segmentation," in *Proc. Int. Workshops Image Video Technol. (PSIVT)*, Sydney, NSW, Australia. Cham, Switzerland: Springer, 2020, pp. 162–171.

[50] M. A. Shirazi and L. Boersma, "A unifying quantitative analysis of soil texture," *Soil Sci. Soc. Amer. J.*, vol. 48, no. 1, pp. 142–147, Jan. 1984.

[51] O. Ronneberger, P. Fischer, and T. Brox, "U-Net: Convolutional networks for biomedical image segmentation," in *Proc. 18th Int. Conf. Med. Image Comput. Comput.-Assist. Intervent. (MICCAI)*, Munich, Germany. Cham, Switzerland: Springer, Oct. 2015, pp. 234–241.

[52] H. Zhao, J. Shi, X. Qi, X. Wang, and J. Jia, "Pyramid scene parsing network," in *Proc. IEEE Conf. Comput. Vis. Pattern Recognit. (CVPR)*, Jul. 2017, pp. 6230–6239.

[53] V. Badrinarayanan, A. Kendall, and R. Cipolla, "SegNet: A deep convolutional encoder-decoder architecture for image segmentation," *IEEE Trans. Pattern Anal. Mach. Intell.*, vol. 39, no. 12, pp. 2481–2495, Dec. 2017.

[54] L.-C. Chen, Y. Zhu, G. Papandreou, F. Schroff, and H. Adam, "Encoder-decoder with atrous separable convolution for semantic image segmentation," in *Proc. Eur. Conf. Comput. Vis. (ECCV)*, 2018, pp. 801–818.

[55] M. Das and A. Bais, "DeepVeg: Deep learning model for segmentation of weed, canola, and canola flea beetle damage," *IEEE Access*, vol. 9, pp. 119367–119380, 2021.

[56] H. S. Ullah, M. H. Asad, and A. Bais, "End to end segmentation of canola field images using dilated U-Net," *IEEE Access*, vol. 9, pp. 59741–59753, 2021.

[57] C. Szegedy, V. Vanhoucke, S. Ioffe, J. Shlens, and Z. Wojna, "Rethinking the inception architecture for computer vision," in *Proc. IEEE Conf. Comput. Vis. Pattern Recognit. (CVPR)*, Jun. 2015, pp. 2818–2826.

[58] M. Tan and Q. V. Le, "EfficientNet: Rethinking model scaling for convolutional neural networks," *Proc. 36th Int. Conf. Mach. Learn. (ICML)*, vol. 97, 2019, pp. 6105–6114. [Online]. Available: http://proceedings.mlr.press/v97/tan19a.html

[59] C. E. Shannon, "A mathematical theory of communication," *Bell Syst. Tech. J.*, vol. 27, no. 3, pp. 379–423, Jul. 1948.
[60] R. D. Grisso, M. M. Alley, D. L. Holshouser, and W. E. Thomason, "Precision farming tools. Soil electrical conductivity," Virginia Cooperat. Extension, Blacksburg, VA, USA, Tech. Rep. 424-014, 2005.
[61] *Cropwatch*, United States Dept. Agricult., Natural Resour. Conservation Services (USDA-NRCS), U.K., nos. 1–9, May 2014.
[62] M. Fourie, "What can electrical conductivity tell us about our soil," Trace Save, Tech. Rep. 905, 2017.

EKUNAYO-OLUWABAMI BABALOLA received the B.Sc. degree in electrical engineering from Covenant University, Ota, Nigeria, in 2019. She is currently pursuing the M.Sc. degree in electronic systems engineering with the University of Regina. Her research interests include computer vision, machine learning, and artificial intelligence. She is improving image labeling solutions for agricultural data and analyzing agricultural images for soil properties, such as texture and organic matter for improved field management.

MUHAMMAD H. ASAD (Graduate Student Member, IEEE) received the B.Sc. degree in electrical engineering from the University of Engineering and Technology, Lahore, Pakistan, in 2009, and the M.Sc. degree in electronic systems engineering from the University of Regina, Saskatchewan, Canada, in 2019, where he is currently pursuing the Ph.D. degree in electronic systems engineering. His research interests include signal processing, machine learning, and artificial intelligence algorithms, with a special focus on precision agriculture. He is also working on applications of AI in variable rate technology in site-specific management of agriculture fields. It includes monitoring crops and weeds and mapping soil attributes like texture and organic matter.

ABDUL BAIS (Senior Member, IEEE) received the M.Sc. degree in electrical engineering from the University of Engineering and Technology, Peshawar, Pakistan, in 2003, and the Ph.D. degree in electrical engineering and information technology from the Vienna University of Technology, Vienna, Austria, in 2007. From 2010 to 2013, he was a Postdoctoral Fellow with the Faculty of Engineering and Applied Science, University of Regina, Saskatchewan, Canada, where he is currently an Associate Professor with the Faculty of Engineering and Applied Science. He is also a Certified Instructor with the NVIDIA Deep Learning Institute and a Licensed Professional Engineer in Saskatchewan. His research was supported by the Natural Sciences and Engineering Research Council of Canada (NSERC Alliance and Discovery Programs), Mitacs (www.mitacs.ca), the Saskatchewan Ministry of Agriculture, and the AgTech industry. His research interests include deep learning/machine learning, data analysis, image processing, and computer vision.